Chapter 1
INTRODUCTION

BACKGROUND

The goal of this thesis is to describe the measurement of atmospheric aerosol in an Arctic environment and to place these measurements in perspective within the discipline of atmospheric physics. To achieve this goal a brief overview of aerosol research and the analytical tools needed to analyze the data will be presented. The design, implementation and calibration of the narrow-band filter radiometers, broad band pyrheliometer and the CCD fiber optic spectrometer will be described. Data were collected primarily at Thule Air Base (Pituffik), Greenland, at 76.5°N about 810 nautical miles (1500 km) from the North Pole. The Arctic aerosol data covers the period from mid May through early October of 1999. The CCD instrument was tested and used in Silkeborg, Denmark, at 56.1°N to gather solar spectra with a view to remote deployment for aerosol measurements in the future.

The increased awareness over the past few decades of anthropogenic and natural phenomena upon the atmosphere has caused increased attention to be focused on the effects of atmospheric aerosols on the Earth's radiation balance. GCM's (*Global Climate Models* or *General Circulation Models*) which can adequately predict changes in the mean temperature of boundary layer air require knowledge of the spatial distribution, constituents, concentration and size distribution of tropospheric aerosol particles. This thesis describes optical techniques for obtaining some of this information and instrumentation for performing the measurements. The Arctic experiments in Pituffik were carried out at the DMI (*Danish Meteorological Institute*) research facility located near Thule Air Base (76.5°N, 68.8°W).

The radiation balance of the Earth is affected by atmospheric aerosols, small particles typically ranging in diameter from about 0.01 μm to 20 μm. Aerosol effects can be *direct* due to scattering and absorption of incident solar and reflected terrestrial radiation or *indirect* due the important role played by aerosols in cloud formation. The total incident solar radiation intensity averaged over the entire surface of the Earth is about 344 W/m^2. The total climatic effect of aerosols and other factors can conveniently be expressed as the *climate forcing* expressed in just these units.

The IPCC (*Intergovernmental Panel on Climate Change*) Working Group report of 1995 suggests that aerosol may cause negative climate forcing of up to 1 or 2 watts per square meter and thus to some extent compensate for global warming effects due to greenhouse gasses ($+2.4\pm0.4$ W/m^2). There are many techniques for performing observations of the spatial, temporal and size distribution of atmospheric aerosol. These methods include observations from satellites, aircraft, balloon-borne instruments and optical observations of the extinction of solar beam radiation performed by instruments on the ground. It is this latter method which is the primary focus of this thesis.

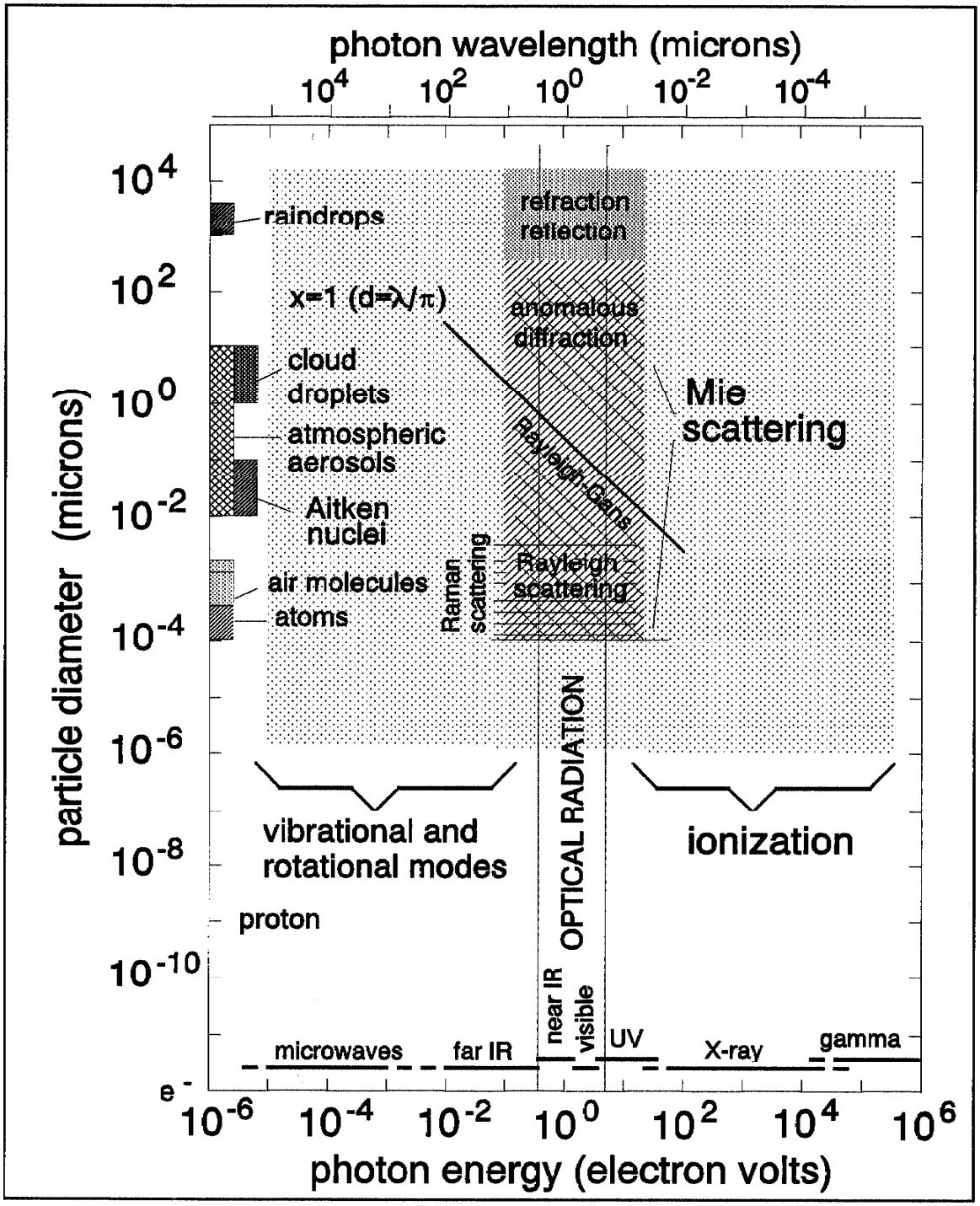

Figure 1.1: *Some important interactions between photons of wavelength* λ *and particles of diameter* d *are shown. Rayleigh scattering applies for values of the size parameter* $x = \pi d/\lambda << 1$, *while van de Hulst's theory of anomalous diffraction is a good approximation to the general Mie theory for* $x >> 1$. *The region of vibrational and rotational excitation and the ionization region overlap in the optical wavelength range.*

RADIATION AND PARTICLES

Figure 1.1 on the facing page shows the extraordinary wealth of phenomena encountered when one considers the interaction of radiation and particles. The figure displays a domain of particle diameters d corresponding to 17 orders of magnitude and a range of wavelengths λ corresponding to 12 orders of magnitude.

The upper left hand corner of the figure corresponds to particle diameters of 10 centimeters and one meter electromagnetic waves in the short wave radio region of the spectrum. At the other extreme in the lower right hand corner one finds 1 MeV gamma radiation and extremely small "particles" such as electrons and positrons, where the concept of particle diameter is no longer well-defined.

An important parameter encountered in the description of interactions between particles and photons is the *particle size parameter* x defined as:

$$x = \frac{\pi \cdot d}{\lambda} \qquad (1.1)$$

and corresponding to the circumference of the particle divided by the wavelength of the incident radiation. For example in the optical region of the spectrum from about 300 nm to 3000 nm (where glass components can be used) the size parameter indicates which of several approaches is appropriate: Mie scattering theory, Rayleigh scattering theory, the Rayleigh-Gans approximation or van de Hulst's theory of anomalous diffraction.

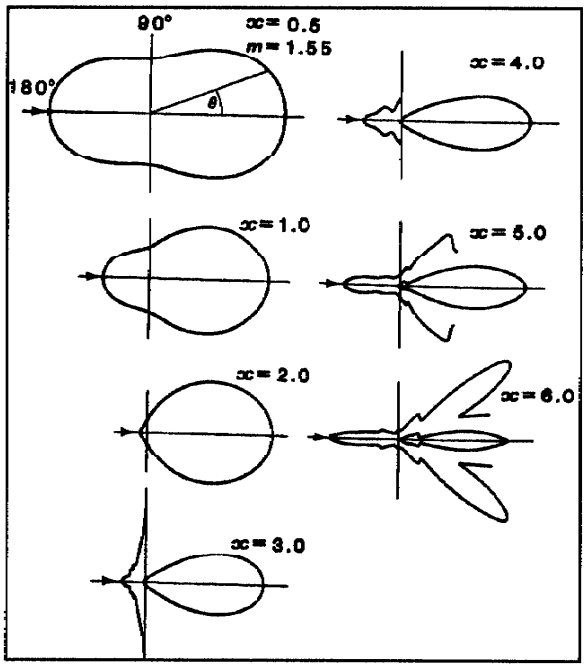

Figure 1.2: *Light scattering. Note that the outer curves magnify the graphs by a factor of 10* [Allen, 1981, p 417].

Rayleigh scattering theory works very well when $x << 1$, i.e. the wavelength of light is much larger than the particle size. When the condition $x < 1$ is fulfilled the Rayleigh-Gans approximation can be used. This is much simpler than using the more general Mie theory which is needed for $x \geq 1$. When $x >> 1$ the theory of anomalous diffraction also permits a somewhat simpler approach to the problem. The theories mentioned here all build upon classical electromagnetic theory, i.e. Maxwell's equations, and yield results in excellent accord with observations within their ranges of validity.

The ability of the physicist to provide an adequate treatment of phenomena encountered in each region of the figure is dictated by the availability of appropriate physical theories and manageable analytical tools. For example, the interaction of dielectric, centimeter-size spheres with centimeter-size microwaves might be handled by

analogy to the theory of Mie scattering, for the particle size parameter x is close to unity. Compton scattering of gamma photons by electrons involves particle sizes substantially smaller than the photon wavelength so that $x << 1$, and it turns out that a treatment using classical electromagnetic theory yields results analogous to Rayleigh scattering of visible light by air molecules. Modifications are necessary, however, because this approach does not properly account for the quantum aspects of light [*Segrè, 1976, pp 51-54*].

The subject this research has been a closer examination of the region in the middle portion of Figure 1.1 encompassing optical wavelengths and including particle sizes in the micrometer range.

RAYLEIGH SCATTERING

Treatments of Rayleigh scattering begin by pointing out that the dielectric sphere assumed to cause the scattering must be much smaller that the incident radiation wavelength λ, so that the phase of the electric field of the monochromatic incident wave will be nearly constant over the particle. It is also customary to assume initially that the incoming wave is linearly polarized.

The electric field creates an electric dipole moment $M = p \cdot E_0$, where p is a constant called the *polarizability* of the particle. Both M and E_0 are sinusoidally varying functions with a period corresponding to the wavelength of the radiation in the medium surrounding the particle. The initial direction of the incident wave and the line of sight from the particle to the observer form a *reference plane*, and the scattering angle Θ is the angle between the direction of incidence and the line from the scattering particle to the observer. The now polarized dielectric particle is set in motion by the field, and by classical electromagnetic theory due to Hertz the oscillating dipole emits a spherical wave with the electric field:

$$E_1(t) = \left(\frac{2\pi}{\lambda}\right)^2 \cdot \frac{|p|}{r} \cdot E_0(t) \tag{1.2}$$

$$E_2(t) = \left(\frac{2\pi}{\lambda}\right)^2 \cdot \frac{|p|}{r} \cdot E_0(t) \cdot \cos(\theta) \tag{1.3}$$

where E_1 is the component normal to the reference plane, and E_2 is the component parallel to the reference plane. The quantity r is the distance from the oscillating dipole to the observer. Notice that E_2 is a function of Θ and that $E_2(\pi/2)=0$, indicating that scattered radiation viewed from the reference plane and perpendicular to the direction of incidence will be strongly polarized. The intensity of the scattered radiation is given by $\mathbf{E}^2$, the magnitude of the Poynting vector, so that the total energy flux per unit time can be calculated:

$$|E|^2 = \tfrac{1}{2} \cdot \left(\frac{16\pi^4 \cdot p^2 \cdot E_0^2}{\lambda^4 \cdot r^2}\right) \cdot (1 + \cos^2\theta) \tag{1.4}$$

Note that the factor $\tfrac{1}{2}$ arises due to the time averaging of the field strength over

the sinusoidal period of oscillation. Denoting the incident beam intensity I_0 and the scattered beam intensity as a function of the scattering angle θ by $I(\theta)$ we can express the result for Rayleigh scattering as follows:

$$I(\theta) = I_0 \cdot \left(\frac{8\pi^4 \cdot p^2}{\lambda^4 \cdot r^2} \right) \cdot (1 + \cos^2\theta) \qquad (1.5)$$

with the first and second terms in the expression $(1 + \cos^2\theta)$ corresponding to the intensities of the vertically and horizontally polarized components respectively.

The combined result for an observer in the reference plane for unpolarized incident light for $x << 1$ is shown in Figure 1.3. Note that the polar plot is similar in appearance to the polar diagram for the smallest value of the size parameter appearing in Figure 1.2 namely $x = 0.5$.

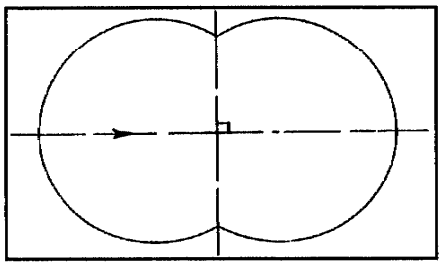

Figure 1.3: *Rayleigh scattering of unpolarized incident light.*

Rayleigh scattering theory provides an excellent approximation for the scattering of visible light ($\lambda \approx 550$ nm) by air molecules ($d \approx 360$ pm) [*Kaye, 1975, p 40*], for here $x \approx 0.002$.

Just to briefly mention some interesting practical consequences of these results:

- The sky appears blue.
- The Sun appears reddish at sunset.
- Light from the blue sky viewed at a 90° angle to the direction of incoming direct solar irradiance is strongly polarized.

Light is scattered by air molecules as it passes through the atmosphere, and the scattering is most pronounced for the shorter wavelengths. For example blue light with a wavelength $\lambda \approx 400$ nm will experience substantially more scattering than red light with $\lambda \sim 710$ nm, since $(710/400)^4 \sim 10$. Viewing the sky away from the Sun one therefore observes predominantly blue light. At sunset the Sun's direct rays must pass through many air masses en route to the observer. Most of the blue light will be scattered, while longer wavelength light will pass through, giving the solar disk a reddish appearance. It is also apparent from the Rayleigh scattering equation that scattered light in the sky viewed at 90° to the direct rays of the Sun will be polarized. This can be readily confirmed by rotating a polarizing filter while viewing points on the arc in the sky at 90° from the Sun.

The polarizability p appearing in the Rayleigh equation can be written more explicitly, for it is due to the properties of the dielectric particles which cause scattering. A number of different expressions have been derived involving macroscopic quantities such as the refractive index m of the gas formed by the particles, the number density n (particles per unit volume) and other variables. One such equation for the polarizability states [*Goody, 1995, p 75*]:

$$p = \frac{1}{2\pi} \left(\frac{m-1}{n} \right) \qquad (1.6)$$

ATMOSPHERIC EXTINCTION

With this background information available it is now possible to demonstrate the connection between Rayleigh scattering by individual air molecules and the well-known *Lambert-Beers' exponential law* describing the attenuation of light passing through air. The removal of energy from the light beam may be due to *absorption*, characterized by the absorption coefficient k_λ, or to *scattering*, characterized by the scattering coefficient s_λ, while *extinction* is the combined effect of scattering and absorption. The units of these coefficients are *area*, and the extinction coefficient $e_\lambda = k_\lambda + s_\lambda$. The probability that scattering will be the process occurring is termed the *single scattering albedo* $a_\lambda = s_\lambda / e_\lambda$. In the discussion which follows we assume that Rayleigh scattering is the only process which occurs.

If e_λ is the extinction coefficient per molecule, then the intensity change dI_λ for light traversing an infinitesimal path length $d\ell$ through a medium with number density n is:

$$dI_\lambda = -e_\lambda \cdot n \cdot I_\lambda \cdot d\ell \tag{1.7}$$

It can be helpful to imagine the extinction process as due to a collision between a photon of negligible size and a molecule for which a collision cross section can be defined, in this case e_λ. Using this idea the mean free path Γ_λ between collisions for a photon is given by:

$$\Gamma_\lambda = \frac{1}{e_\lambda \cdot n} \tag{1.8}$$

To demonstrate the validity of Equation 1.8 one can imagine a one meter long cylinder of air with a base area of one square meter and that a photon passes through it parallel to the axis of the cylinder. What is the chance of a collision? The quantity n tells us how many air molecules are present within this unit of volume. Suppose further that there are so few molecules that the chance of their hiding one another is negligible. The collision area presented to the photon divided by the area of the base of the cylinder is then $n \cdot e_\lambda$ and corresponds to the probability of a collision during this one meter of travel. The reciprocal corresponds to the mean free path as stated in Equation 1.8. For example, if the probability of a collision during one meter of travel is found to be 20%, one would expect a collision on an average of every 5 meters.

To show the connection between Rayleigh scattering from individual atoms or molecules and the macroscopic extinction coefficient in Lambert-Beers' law, we assume that scattering occurs from a single particle so that $n \cdot d\ell = 1$ and that extinction is only due to scattering: $e_\lambda = s_\lambda$. Because s_λ can be interpreted as the probability of a collision with subsequent loss of the photon from the beam, we can write $dI/I = -s_\lambda$ where the minus sign reflects the fact that $dI < 0$. The intensity loss dI is due to scattering into a sphere of radius r surrounding the scattering center. A differential element of area on the surface of this sphere is given by:

$$dA = \pi \cdot (2 \cdot r \cdot \sin\theta) \cdot r \cdot d\theta = 2\pi \cdot r^2 \cdot \sin\theta \cdot d\theta \tag{1.9}$$

The magnitude of the intensity loss $-dI$ must correspond to the integral of the scattered intensity $I(\Theta)$ from Equation 1.5 over the entire sphere:

$$-dI = \int_{sphere} I(\theta)\, dA = \int_o^{\pi} \left(\frac{2\pi}{\lambda}\right)^4 \cdot \frac{p^2}{r^2} \cdot I \cdot \frac{1+\cos^2\theta}{2}\, 2\pi \cdot r^2 \cdot \sin\theta \cdot d\theta \qquad (1.10)$$

$$-dI = \left(\frac{2\pi}{\lambda}\right)^4 \cdot p^2 \cdot \pi \cdot I \cdot \int_o^{\pi} (1+\cos^2\theta) \cdot \sin\theta\, d\theta \qquad (1.11)$$

The integral can readily be evaluated (by using $t = cos\ \theta$ and $dt = -sin\ \theta \cdot d\theta$) and found to be equal to 8/3. Finally we obtain:

$$-dI = \frac{8\pi}{3} \cdot \left(\frac{2\pi}{\lambda}\right)^4 \cdot p^2 \cdot I \qquad (1.12)$$

Comparing this result for $-dI$ with the fact that $-dI = s_\lambda \cdot I$ we can conclude:

$$s_\lambda = \frac{8\pi}{3} \cdot \left(\frac{2\pi}{\lambda}\right)^4 \cdot p^2 = \frac{32 \cdot \pi^3}{3 \cdot \lambda^4} \cdot \left(\frac{m-1}{n}\right)^2 \qquad (1.13)$$

where we have used the expression for the polarizability p from Equation 1.6. The connection sought after has been found.

Let us consider a simple application of this result for light with $\lambda = 550$ nm in pure air at STP (0°C and 1 atm). Recalling that one mole of a gas consisting of 6.022×10^{23} molecules has a volume of $0.0224\ m^3$ at STP, we find that the number density $n = 2.688 \times 10^{25}\ m^{-3}$. The refractive index $m = 1.000292$ for air at STP [*Kaye, 1975, p 87*], so that $s_\lambda \approx 4.265 \times 10^{-31}\ m^2$. Thus the extinction coefficient $s_\lambda \cdot n \approx e_\lambda \cdot n$ in Lambert-Beers' law would be $1.146 \times 10^{-5}\ m^{-1}$. This corresponds by Equation 1.8 to a mean free path $\Gamma_\lambda \approx 87$ kilometers.

Additional simplifications can be introduced e.g. because the index of refraction for gasses is often close to unity, but they will not be pursued further here. Instead we will look at a slightly more complex scattering equation valid when the particle size parameter $\pi \cdot d/\lambda$ increases and approaches unity.

RAYLEIGH-GANS SCATTERING

As particle size increases compared to the wavelength of the scattered radiation, the simplifying assumption that the phase of the incident wave is constant over the particle volume no longer applies. Consequently the angular dependence of the intensity of the scattered light becomes more complex. [*Allen, 1981, p 419*] cites the result:

$$I(\theta) = I_0 \cdot \left[\frac{2\pi^2}{\lambda^4} \cdot V^2 \cdot \frac{(m-1)^2}{r^2}\right] \cdot \left[\frac{3}{u^3} \cdot (\sin u - u \cdot \cos u)\right]^2 \cdot (1+\cos^2\theta) \qquad (1.14)$$

The terms 1 and $\cos^2\theta$ refer again to the vertically and horizontally polarized components respectively, and I_0 is the intensity of the incident radiation. The quantity V is the particle volume and m here refers to the *index of refraction of the spheres*. The particle diameter d now appears explicitly in the scattering equation through the parameter u defined as follows:

$$u = \frac{2\pi \cdot d}{\lambda} \cdot \sin(\theta/2) \qquad \textbf{(1.15)}$$

Notice that the second term in Equation 1.14 contains trigonometric functions of u. Expanding $\sin u \approx u - u^3/6$ and $\cos u \approx 1 - u^2/2$ and reducing one can show that the term is close to unity for small values of u. Note that u will be small for small values of the size parameter $\pi \cdot d/\lambda$ and/or the scattering angle θ. Setting this term equal to one reduces the equation to the Rayleigh scattering formula, Equation 1.5.

By differentiating Equation 1.14 with respect to the parameter u it is possible to discover the conditions for minimum and maximum intensity. When this exercise is carried out, it is turns out that the scattering angles at which extrema occur depend upon particle size and wavelength. Thus a scattering distribution function can reveal information about particle size. Of course a mixture of many different particle sizes and wavelengths complicates the situation and makes the extraction of particle size information difficult. Techniques for achieving this, e.g. for examination of particle sizes in a controlled industrial environment, are reviewed by Allen [*1980, p 420*].

We proceed now to consider the most general theory for the scattering of optical radiation by particles, the Mie scattering theory.

MIE SCATTERING

A complete review of the Mie theory of scattering is available in the work of van de Hulst [*1954*]. Only the fundamental results are reviewed here based upon the overviews provided by McCartney [*1976, p 228*] and Goody [*1995, p 71*]. The theory applies to all particle sizes and wavelengths, and the main results are based on two intensity distribution functions denoted by i_1 and i_2. These components are proportional to the components of the scattered beam irradiance $I_\perp(\theta)$ and $I_{//}(\theta)$ perpendicular to and parallel to the plane of observation respectively.

$$i_1(x,m,\theta) = \left|\Sigma_{k=1}^{\infty} \frac{2k+1}{k\cdot(k+1)} \cdot (a_k \cdot \pi_k + b_k \cdot \tau_k)\right|^2 \qquad \textbf{(1.16)}$$

$$i_2(x,m,\theta) = \left|\Sigma_{k=1}^{\infty} \frac{2k+1}{k\cdot(k+1)} \cdot (a_k \cdot \tau_k + b_k \cdot \pi_k)\right|^2 \qquad \textbf{(1.17)}$$

k is a dummy variable, x is the size parameter, m is the particle refractive index and θ is the scattering angle in the reference plane defined earlier. The functions π_k and τ_k depend only upon the scattering angle θ and involve first and second derivatives of Legendre polynomials of order k and with argument $\cos\theta$. The coefficients a_k and b_k are found from Ricatti-Bessel functions whose arguments are formed from the particle characteristics x and m but independent of the scattering angle. Extensive tabulations

of these functions and coefficients are available in the literature [*McCartney, p 230*]. Each series in Equations 1.16 and 1.17 converges slowly, and when $x > 1$ the number of terms needed for good convergence is somewhat greater than the value of x. When $x << 1$ the first term in each series corresponds to Rayleigh scattering. Note that each series is defined for incident polarized light of unit irradiance.

For a particle illuminated by unpolarized, incoherent light the scattered light consists of two incoherent components:

$$I(\theta) = \frac{I_{\perp}(\theta) + I_{//}(\theta)}{2} = E \cdot \frac{\lambda^2}{4\pi^2} \cdot \left(\frac{i_1 + i_2}{2} \right) \qquad (1.18)$$

where E is the magnitude of the electric vector of the incident light.

Figure 1.4 shows a number of intensity distribution functions i_1 and i_2 for small, nonabsorbing spheres with real refractive index $n = 1.33$ (e.g. water) for $\lambda = 550$ nm. The range of size parameter x covered is from $x = 0.5$ to $x = 5$ corresponding to particle diameters from $d = 0.088$ μm (large Aitken nuclei) to $d = 0.88$ μm (small cloud droplets). Note that the case of particles which also *absorb* radiation is treated by using an index of refraction which is a complex number [*McCartney, 1976, p 225*].

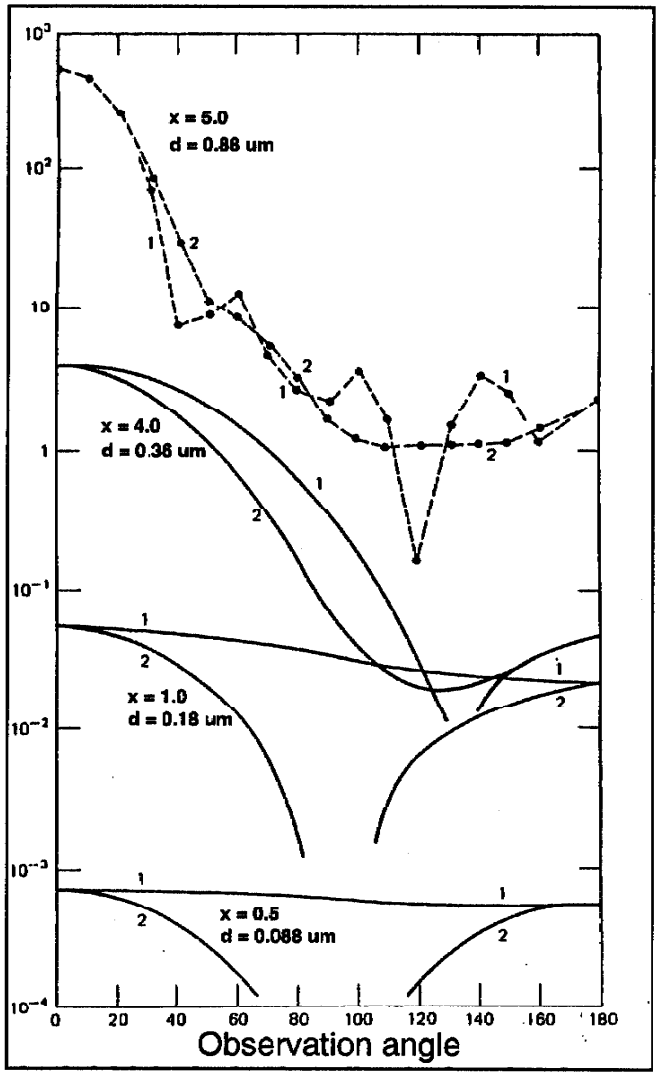

Figure 1.4: *Intensity functions* i_1 *and* i_2 *for nonabsorbing spheres with refractive index* n = 1.33 *(water)* [McCartney, p 232].

Note that for the smallest values of x the scattering functions are similar to the Rayleigh scattering components. The scattering function i_1 corresponding to the first term in the expression $(1 + \cos^2\theta)$ is nearly independent of the scattering angle, and the scattering function i_2 displays an angular dependence like $\cos^2\theta$ with a very small value at $\theta = 90°$. As particle size increases, forward scattering exceeds backscattering as can also be seen from Figure 1.2. The complexity of the scattering functions increases with increasing particle size with many extrema appearing. Note also that the graphs of i_1 and i_2 are always equal for angles $\theta = 0°$ and $\theta = 180°$. For other observation angles the light will be partially polarized. The *degree of polarization* P is defined as:

$$P = \frac{i_1 - i_2}{i_1 + i_2} \qquad (1.19)$$

It is interesting to note the dramatic changes in the scattering functions which occur as particle size increases from ca. 0.1 μm to 1.0 μm. This might occur when water vapor condenses on Aitken nuclei which grow in size as the temperature falls and relative humidity increases in the evening hours. Maximum scattering for a given volume of water occurs when the water forms drops which are the same order of size as the incident radiation wavelength.

From Figure 1.4 it is clear that fog droplets ($\approx$ 1 μm) are much more effective scatterers of light than water vapor or haze droplets ($\approx$ 0.1 μm). Cloud droplets (about 0.5 to 10 μm) are very effective at scattering incident light. Notice that when flying through cloud in an aircraft it is sometimes impossible to see the wingtips just a few meters away due to the dramatic extinction of light causes by cloud droplets. It is also important to realize that during unstable periods with high relative humidity, changes in the droplet size can cause visibility to deteriorate dramatically within a short period of time: an important piece of safety information for pilots and sailors.

ANOMALOUS DISPERSION

For larger particle sizes ($x >> 1$) van de Hulst's theory of anomalous diffraction can be applied. It was developed in the late 1950's based on principles from physical optics. Van de Hulst assumed that $m - 1 << 1$ where m is the index of refraction of the dielectric spheres.

A basic parameter of this theory is the *normalized size parameter* ρ defined as:

$$\rho = 2x \cdot (m-1) = \frac{2\pi \cdot d}{\lambda} \cdot (m-1) \qquad (1.20)$$

which links the three fundamental particle scattering parameters: the size parameter x, the radiation wavelength λ and the index of refraction m. For radiation in the visible and near infrared (NIR) region of the spectrum the theory applies to fog and cloud droplets with diameters greater than a few microns.

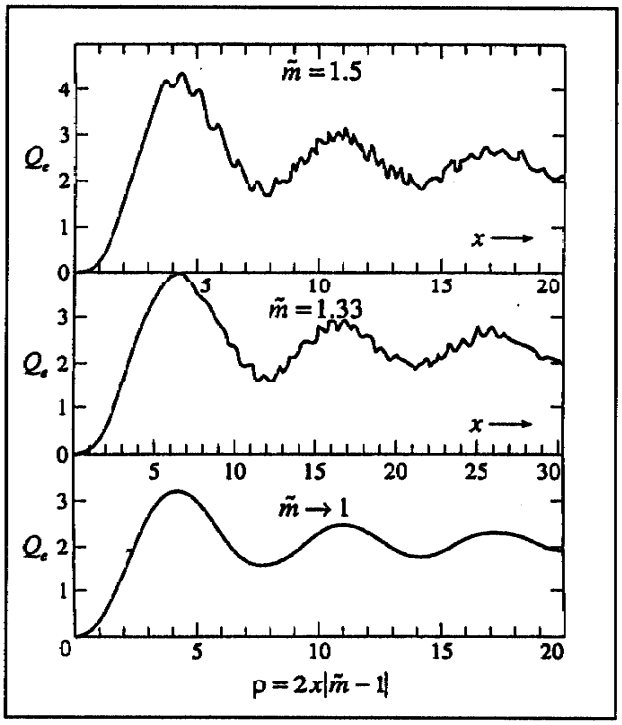

Figure 1.5: *This classic illustration due to van de Hulst shows scattering efficiencies of large dielectric spheres* [Goody, p 80].

The scattering efficiency Q_S is an important quantity in this connection. It is defined at the ratio of the scattering coefficient s_λ to the geometric cross sectional area of the sphere $\pi \cdot d^2/4$. A scattering efficiency factor of unity would thus mean that a photon will be scattered if it strikes within the geometric area of the disc presented by the sphere. It is the scattering

efficiency which is displayed in Figure 1.5 for a range of values of m as a function of the normalized size parameter. Note that the top two panels are Mie theory calculations and the lower panel is the approximation for the scattering efficiency derived from the theory of anomalous diffraction (Equation 1.22).

The theory is developed by considering incident rays of light striking a droplet. The index of refraction must be assumed to be close to unity so that reflection from the air – droplet interfaces and refraction effects are negligible. The phase of the wave passing through the drop will depend upon the optical path which it traverses. It can be shown that the phase lag δ in radians due to the light ray entering the drop at different points is given by:

$$\delta = d \cdot \sin\tau \cdot (m-1) \cdot \frac{2\pi}{\lambda} = \rho \cdot \sin\tau \qquad (1.21)$$

where τ is the angle measured from the normal to the central ray through the center of the drop and the point on the sphere were a given ray enters. The *phase lag* at some point P at some distance beyond the drop is equal to the parameter ρ defined in Equation 1.20. Light not passing through the drop but which is diffracted around the drop will not experience any phase lag. If this light reaches the same point P the sort of interference which occurs there will depend upon the phase lag ρ.

On this basis and considering only scattering processes and no absorption van de Hulst's theory leads to the result:

$$Q_e = 2 - \frac{4}{\rho} \cdot \sin\rho + \frac{4}{\rho^2} \cdot (1 - \cos\rho) \qquad (1.22)$$

It is this scattering efficiency which is displayed in the lower panel of Figure 1.5. An expression for the total extinction efficiency due to absorption as well as to scattering can also be derived [*McCartney, 1976, p 258*]. Although not clearly apparent in Figure 1.5 there is not good agreement for size parameter values $x << 1$. For larger values of x the theory of anomalous diffraction does provide a good overall picture of extinction by dielectric spheres even for refractive indices quite different from one. As pointed out by Goody [*1995, p 81*] the theory fails to reproduce the fine structure shown by the Mie theory. However, because of the mixture of sizes occurring in natural aerosols, the fine structure is often unimportant in atmospheric applications.

The wavy structure visible for larger values of x (and thus of ρ) in Figure 1.5 is due to interference between the light which is transmitted through the particles and the light diffracted around them. Notice that the separation $\Delta\rho$ between successive maxima is about 2π. For large values of x (for $\rho > 10$) Q_e no longer varies so much, implying that scattering for this range of particle sizes is not strongly dependent on wavelength. (If wavelength changes were important, changes in λ for a given particle diameter d would cause ρ to vary and cause Q_e to change.) The fact that clouds appear white is thus due to anomalous diffraction, while the bluish appearance of the sky is due to Rayleigh scattering.

A log-log plot of Q_e instead of the linear plot shown in Figure 1.5 would show that the slope of the graph is close to 4 for small values of ρ. For constant particle size this reveals the λ^{-4} dependence to be expected in a region where Rayleigh scattering theory

is applicable. At the other extreme notice that Equation 1.22 clearly indicates that in the limit of large particles where $\rho \rightarrow \infty$ the scattering efficiency factor $Q_e \rightarrow 2$, and this fact is also apparent from Figure 1.5. A few remarks are appropriate concerning why the large particle classical optics limit of Q_e has just this value.

If only light intercepting the disc of diameter d were scattered, then the scattering cross section s_λ would be the same as the geometric cross section, and Q_e would be equal to unity. Values of Q_e greater than one suggest that the particle affects the electromagnetic field beyond its geometric area. A qualitative argument that Q_e should be 2 in the large particle limit can be gleaned from *Babinet's principle* which states that an aperture and the corresponding opaque object produce complementary diffraction patterns. The diffraction effects plus the reflection and refraction of the light striking the geometric cross section turns out to cause $Q_e = 2$. A more complete discussion of this interesting question is available in McCartney [*1976, p 250*].

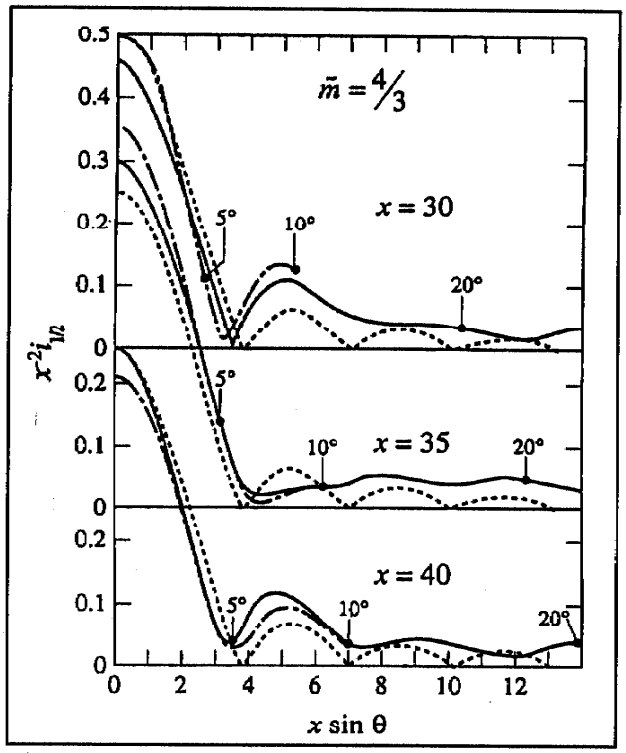

Figure 1.6: *The unbroken graphs correspond to exact (Mie) calculations, the dash-dot lines to anomalous diffraction and the dotted lines to Fraunhofer diffraction.*

Figure 1.6 illustrates the correspondence between the theory of anomalous diffraction, the exact Mie theory and the Fraunhofer patterns familiar from diffraction studies in physical optics. The unusual notation on the ordinate axis is due to Goody [*1995, p 81*] and is intended to mean i_1 or i_2 divided by x^2. The strong forward scattering peak associated with large particle scattering is clearly revealed in Figure 1.6.

EXTRATERRESTRIAL SOLAR SPECTRAL IRRADIANCE

The light source used in the aerosol studies described in this thesis is the Sun itself. It is therefore essential to have a clear understanding of the spectral and temporal properties of the irradiance reaching the Earth. Although there is some evidence in the literature that there may be small variations in the radiation emitted by the Sun due to sunspot activities, we will for the purposes of this work assume that these variations are of minor importance. The uncertainty which persists regarding possible variations in the solar constant may be due to degradation in the optical properties of filters and other optical components in the Nimbus 7 satellite after an extended period in the extremes of space [*Hickey, 1982*].

Figure 1.7 shows the extraterrestrial solar spectral irradiance at the mean Earth-Sun distance. Most of the solar radiation reaching the Earth is emitted from the outer 500 km

of the solar surface, the *photosphere*. The observed spectral irradiance reaching the Earth closely follows the Planck radiation law, i.e. the radiation observed from a perfect blackbody at an absolute temperature $T = 5777$ K with maximum emission in the visible region close to 500 nm.

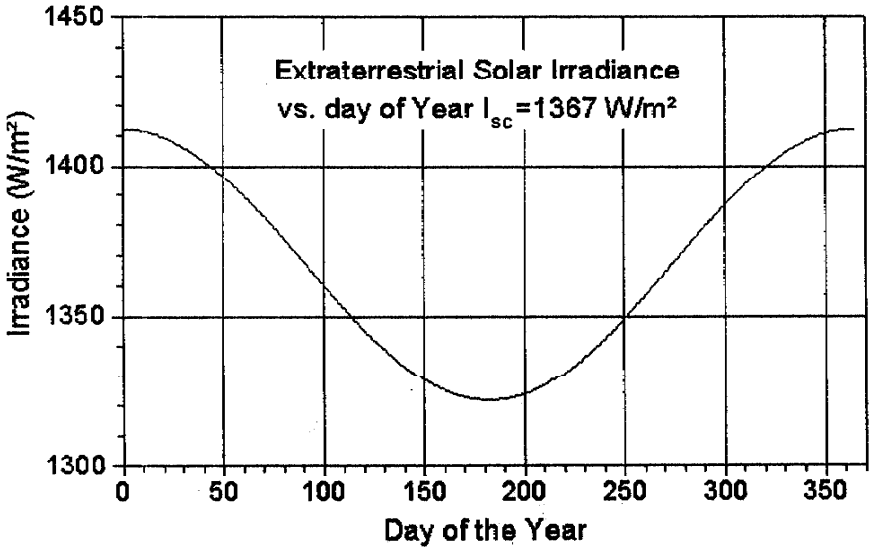

Figure 1.7: *Solar spectral irradiance at the mean Sun-Earth distance (Goddard Space Flight Center, Greenbelt, MD, USA).*

By comparison the Earth with an average surface temperature around 300 K emits like a blackbody radiator with a peak radiant exitance at about 10 μm [*Seinfeld, 1998, p 26*].

Careful observations of variations in the Earth-Sun orbital distance make it possible to describe the value of the extraterrestrial irradiance on a given day of the year. The following algorithm can be applied to compute the solar spectral irradiance used in connection with the interpretation of optical depth measurements.

$$I_0 = I_{SC} \cdot [1 + 0.033 \cdot \cos(2\pi \cdot \{N-3\}/365)] \qquad \textbf{(1.23)}$$

where N is the day number counting from January 1st, and $I_{SC} = 1367$ W/m² is the value of the *solar constant*. Note that I_0 is at a maximum at the Earth orbit perihelion on January 3rd and at a minium at aphelion half a year later. This fact moderates winters and summers in the Northern Hemisphere compared with corresponding southern latitudes. The extraterrestrial solar irradiance variation is shown graphically in Figure 1.8.

The direct solar spectral irradiance reaching an observer on the surface of the Earth depends upon the properties of the intervening atmosphere and the path traversed by the incident radiation. For a clear atmosphere with no visible water vapor, radiation normally incident from space will pass through a unit air mass (abbreviated AM1). For non-normally incident radiation, the usual situation in practice, the air mass must be evaluated for the atmospheric component of interest. Algorithms exist for finding the air mass for the primary atmospheric components (oxygen and nitrogen) as well as for

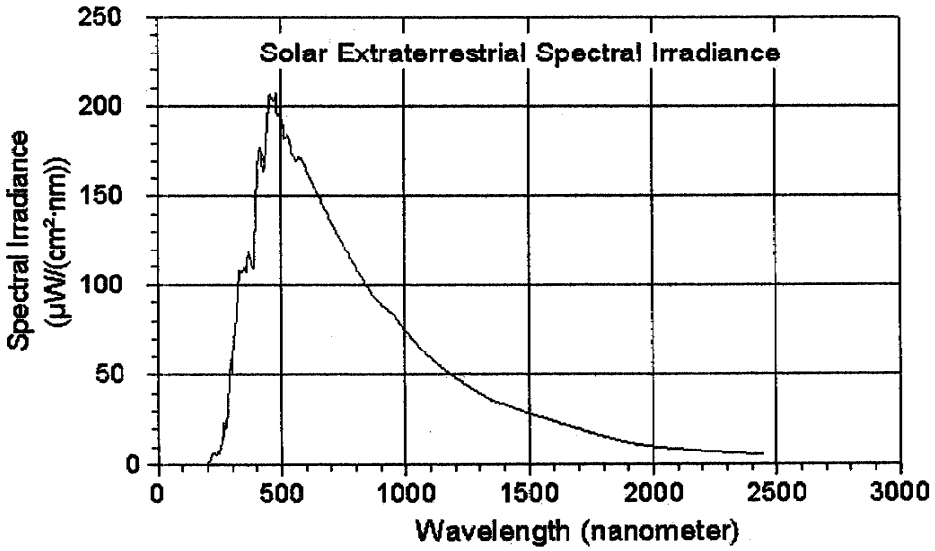

Figure 1.8: *There is a slight change in the extraterrestrial solar irradiance during the year due to the elliptical orbit of the Earth around the Sun.*

important minor constituents such as ozone and NO_2 which are present in layers high in the stratosphere.

When the air mass is known, extinction can be calcutated on the assumption that the Lambert-Beers attention law $I = I_0 \cdot exp(-\Sigma_i \tau_i \cdot m_i)$ is valid, where I_0 is the intensity of the source, I is the observed intensity, τ_i is the optical depth of the atmospheric constituent, and m_i is the corresponding air mass. Extinction will occur due to absorption at particular wavelengths by components such as oxygen, nitrogen, water vapor, carbon dioxide, ozone and oxides of nitrogen, and Rayleigh scattering will occur due to the interaction of the incident radiation and air molecules.

Measurements of atmospheric extinction to reveal aerosol optical depths are made in portions of the solar spectrum without significant molecular absorption. If atmospheric aerosols are present, extinction due to these small particles will also affect the spectral irradiance. Our task involves taking account of all known atmospheric components to thereby reveal the extinction due to atmospheric aerosols.

SUMMARY

In this chapter we have considered a range of scattering processes relevant to the central region of Figure 1.1 when radiation interacts with small particles. The basic properties of the primary light source to be used with this work, the Sun itself, have been briefly mentioned. In Chapter 2 attention will be directed to atmospheric aerosols in general and more specifically how they can be studied by means of ground-based optical instruments. Instrumentation and analytical tools for computing particle size distributions will be described in Chapters 3 and 4 respectively. The actual measurements and their analysis will be the subjects of Chapters 5 and 6.